Bearingless Rotor Aeromechanical Stability Measurements and Correlations Using Nonlinear Aerodynamics

James M. Wang* Inderjit Chopra†

Center for Rotorcraft Education and Research
Department of Aerospace Engineering
University of Maryland
College Park, Maryland 20742

Abstract

The aeromechanical stability of a 1/8th Froude scaled bearingless rotor model was investigated experimentally in a wind tunnel. Both shaft-fixed and shaft-free conditions were examined to study the aeroelastic stability of a bearingless rotor without the incorporation of auxiliary dampers. This wind tunnel investigation generated a set of stability data for four different advance ratios, and a wide range of collective pitch settings. Theoretical analysis was performed using the newly developed **University of Maryland Advanced Rotorcraft Code (UMARC).** For analysis, the blade is modeled as an elastic beam undergoing flap bending, lag bending, elastic twist, and axial deformation. Blade response is calculated using a finite element method in time. Nonlinear aerodynamic effects are included by using a semi-empirical stall modeling. The linearized periodic rotor perturbation equations in the nonrotating frame are solved for stability roots using Floquet transition matrix theory, as well as constant coefficient approximation. The predicted results are compared with the experimental data.

Introduction

In recent years there has been growing interest in bearingless rotors because of design simplicity, better maintenance, suitability to aeroelastic tailoring, and to improve handling qualities. A bearingless rotor is one special example of a hingeless rotor in which the flap and lag hinges as well as the pitch bearings are eliminated. The distinguishing feature of the bearingless rotor is a torsionally soft flexbeam located between the blade and the hub. Pitch control to the main blade is applied through a torsionally stiff torque tube by rotating the tube with pitch link, which in turn twists the flexbeam. To achieve manageable bending stresses on the flexbeam, bearingless rotors are designed as soft-inplane rotors. However, the soft-inplane rotor is more prone to bending-torsion coupling. For soft-inplane rotor, the low-frequency regressive lag mode may coalesce with the fuselage modes to cause air or ground resonance instability. For articulated rotors, the instability problems are taken cared by adding mechanical lag dampers. Since there is no lag hinge on bearingless rotors, lag dampers are less effective. Thus, there is a need to determine precisely the aeromechanical stability of bearingless rotors at different flight conditions.

The analysis of a bearingless rotor system is more involved than that of a hingeless or an articulated rotor system because of redunancy of load paths at the blade root. In addition, bearingless rotors achieve pitch change through elastically twisting and bending the flexbeam, thus bending-torsion coupling must be treated in a more careful manner. There have been many studies on the the aeromechanical stability of hingeless rotors. However, limited work has been to examine the aeromechanical stability of bearingless rotors. Due to redundancy in load paths and non-

*Graduate Research Assistant

†Professor

[0]Paper presented at the Sixteenth European Rotorcraft Forum, 18th-21st September, 1990.

linear structural couplings, routinely used method of modeling the hingless rotor with rigid blade and springs at the equivalent hinge offset can not be trusted. Most of the previous theoretical work on bearingless rotor aeromechanical stability have been limited to hover because forward flight complicates the analysis by requiring solving nonlinear equations with periodic coefficients. Furthermore, in forward flight the aeroelastic problem is coupled to the trim state of the helicopter, thus both the nonlinear blade response and nonlinear trim equations need to be solved simultaneously.

One of the earliest theoretical works on bearingless rotor was by Hodges [1]. Hodges developed the FLAIR analysis for coupled rotor-body stability of rotorcraft with bearingless blades. The flexbeam was treated as an elastic Euler-Bernoulli beam, and the blade was assumed to be rigid. Simple uniform strip theory aerodynamics was used. Since it was only a hover analysis, the linearized equations are homogeneous ordinary differential equations with constant coefficients. FLAIR was used by Dawson [2] to correlate wind tunnel test results of an isolated bearingless rotor model. Good correlations were achieved for five bearingless rotor configurations. Using FLAIR, Hooper [3] carried out a parametric study of various design parameters, such as precone, and sweep of the flexbeam on aeromechanical stability in hover. It was concluded that a soft-inplane bearingless rotor with no stabilizing design features (i.e. with no flap-lag-torsion couplings introduced by beam installation or other means) is stable in air resonance at low collective and/or low RPMs, but unstable at high collective at operating RPM. Hooper concluded negative pitch-lag coupling is effective at stabilizing air resonance at high collective pitch.

Sivaneri and Chopra [4] developed a refined bearingless rotor hover analysis, based on finite element approach, which included the redundant load paths at the hub, and modeled the blade, fleaxbeam, and torque tube as elastic beam elements. The analysis used a 15 degree of freedom element and solved the finite element equations directly to obtain the blade steady response. Blade stability was calculated from perturbation equations transformed to the normal mode space. Hodges et al [5] later developed another hover code, the GRASP (General Rotorcraft Aeromechanical Stability Program) to include elastic blade modeling for general rotor designs, including bearingless rotors.

Panda and Chopra [6,7] extend the finite element hover code to include aeroelastic stability analysis of composite and hingeless rotor in forward flight. Bir [8] enhanced the model to include the effects of fuselage interaction dynamics. This rotor-fuselage model was later adopted by Jang [9,10] to study air and ground resonance analyses of bearingless rotors. Wang et al [11] conducted shaft-fixed aeroelastic test of Boeing ITR (Integrated Technology Rotor) bearingless rotor in wind tunnel and performed correlations in hover and forward flight. The effects of pitch link stiffness and pitch-lag coupling were examined both experimentally and theoretically. It was concluded that neagtive pitch-lag coupling can help stabilize bearingless rotor. Using the same analysis, Wang and Chopra [12] carried out a parametric study of various design paramters on hingeless rotor aeromechanical stability in hover and forward flight.

While structural dynamic modeling has now advanced to a good level of maturity, the development of computationally efficient and accurate aerodynamic models has lagged behind. In most instances, the rotor dynamicist used simple quasi-steady aerodynamic modeling to keep the computation requirements within manageable limits. Unfortunately, this can severely limit the range of applicability and accuracy of the rotor analysis code. Recently, the finite element aeroelastic analyses used by many researchers [4,6,7,8,9,10,11] were integrated with the aerodynamic work of Torok [13], and further enhenced into a more comprehensive rotor analysis code called the UMARC [14]. The UMARC can perform aeroelastic and aeromechanical analyses of articulated, hingeless, and bearingless rotors in hover as well as forward flight. The aerodynamic capability includes quasi-steady aerodynamics, steady stall, dynamic stall, dynamic inflow, prescribed wake, and free wake models. In the present paper, the results from UMARC are compared with the recent bearingless rotor aeromechanical test conducted at Maryland.

The present paper describes the results from a new aeromechanical stability test of a 1/8th Froude scaled Boeing ITR bearingless rotor model conducted at University of Maryland's Glenn L. Martin Wind Tunnel in January 1990. For this test, a new two degree of freedom gimballed model rig was built.

Stability data are obtained for both shaft-fixed and shaft-free conditions. The objective of the work is to provide a new and much needed data base which can be used by the helicopter community to assess the aeromechanical stability of a bearingless rotor in hover and forward flight. Also, the tests are designed to confirm that a full-scale rotor configuration with adequate aeromechanical stability margin can be built. This data was also used to validate the capability of the UMARC

Description of the Experiment

The experiments were performed in the 8 by 11 foot (2.46 by 3.38 meter) Glenn L. Martin Wind Tunnel at the University of Maryland using a 6 foot (1.85 meter) diameter four bladed bearingless rotor. The model rotor is shown in Figures 1 and 2. The rotor was fabricated by Boeing Helicopter Company under the ITR program. The rotor is a 1/8th Froude scaled dynamic model of a full-scale rotor design under consideration. The design consists of a single flexbeam with a wrap-around type torque tube and a vertical offset of the cuff snubber attachment point. Each of the four flexbeams is instrumented with strain gauges to detect flap and lead-lag responses. The torque tubes are also instrumented with strain gauges to provide torsion response signals. The signals are transmitted from the rotating frame to the fixed frame through a 60 channel slip ring. The signals are then fed through A/D converters and stored on HP1000 computer for both real time processing and future analysis. The geometric characteristics of the rotor are summarized in Table 1.

The model is mounted on a two degree of freedom gimbal system that permits pitch and roll motions. However, steel cantilever springs were added to simulate body pitch and rolling mode stiffness for ground and air resonance study. The model rotor rig has a grabbing mechanism that can grab on to the floating model rotor rig and thus eliminates the body pitch and roll motions (this is called shaft-fixed condition). Or the grabbing mechanism can be released (this is called shaft-free condition). The wind tunnel test results presented here are from the first time this new gimballed rotor rig has been tested. To avoid any potential problem, stiff pitch and roll springs were utilized. The test results show the model is stable at all of the test conditions. In future, the stiff springs will be replaced by very soft springs to better simulate the free flight condition to the air resonance stability.

The entire helicopter model is mounted on a six component balance that can measure three forces and three moments, i.e., lift, two side-forces, and pitching, rolling and yawing moments. The six component balance is itself attached to a mounting pedestal six feet high from the tunnel floor structure. The mounting pedestal has a single degree of freedom pivot that allows the model helicopter pitch angle to be varied at angles of up to $\pm$ 20 degrees to simulate forward flight or rearward flight. The tilt angle is controlled by an external hydraulic actuator attached to the rigid post. A 40 Hp hydraulic motor drives the rotor through a belt transmission. Collective and cyclic pitch inputs are achieved by computer controlled electro-hydraulic servo actuators which have a bandwidth of 0–40 Hz. The complete bearingless model rotor rig was designed inhouse. A schematic of the model rotor rig is shown in Figure 3.

An unique feature of this particular bearingless rotor design is the lag pin shown in Figure 2. This lag pin introduces a kinematic negative pitch-lag coupling (lag back causes nose up) to help stabilize the low-damped lag mode. As illustrated in Figure 4, lag motions result in a horizontal shear reaction at the offset pivot which, together with the opposite shear in the flexure, produces a feathering torque, M_θ. Consequently, M_θ would induce a pitch change if permitted by control flexibility. Two sets of pitch links were used in the previous wind tunnel tests [11] (June 1988) to study quantitatively the significance of control flexibility on pitch-lag coupling and aeroelastic stability. Solid aluminum rod pitch links were used for the stiff pitch link configuration. For the soft pitch link configuration, the stiffness was reduced by incorporating a circular ring of 0.01 inch thick spring steel in the middle of the pitch link. The results presented in Ref. [11] show that soft pitch link permits pitch-lag coupling which in turn helps stabilize the lag mode at advance ratio below 0.35. At higher advance ratio, soft pitch link destabilizes the lag mode slightly. Therefore, both experiment and theoretical results confirm that negative pitch lag coupling can be an effective way to enhance lag mode stability of bearingless rotors. For the ITR bearingless design shown here, the benefit of negative pitch lag coupling through the use of shear pin can only be realized if there exists some flexibility in the pitch link or control system. In the aeromechanical test presented here, rigid pitch links were used because the focus was to examine aeromechanical stability without any stabilizing mechanism.

The model blades used for the wind tunnel tests were obtained from the Boeing Helicopter Company. The blades have $-6°$ of linear twist from the blade/flexbeam junction to the blade tip. Unique to this bearingless rotor design is a 14° pretwist at the blade/flexbeam junction to help reduce the steady state torsional strain in the flexbeam. Thus, under normal flight conditions when the collective pitch is 10° at the 3/4 span, the flexbeam will be at 0° and untwisted. The blade/flexbeam/torque tube twist distribution for this model is illustrated in Figure 5.

The model blades, flexbeams, and torque tube stiffnesses and mass properties were carefully measured to generate input data for theoretical calculations. The flapwise and lead-lag stiffnesses were deduced using a laser system to measure the slope $w'(x)$

of the deflected blade, flexbeam, or torque tube under a prescribed load. The measured slope deflections were curve fitted with cubic splines. The fitted cubic spline expression was differentiated to get $w''(x)$. Since the applied load was known, the bending stiffness EI could be determined using the bending moment relationship $M(x) = EIw''(x)$.

A torsional load was also applied to the blade, the flexbeam and the torque tube independently. Using the reflected laser beam from the deflected blade under tip torque, an accurate angular twist distribution $\theta(x)$ was determined. Then $\theta(x)$ was curve fitted with a cubic spline and the fitted expression differentiated to get $\theta'(x)$. Torsional stiffness for each component were then determined using the torque relationship $Q(x) = GJ\theta'(x)$. Due to poor manufacturing tolerance, the mass and stiffness distributions among the four blades vary by as much as 20%. Due to the blade-to-blade dissimilarity, the experimentally measured lag mode damping for more than one blades are shown in Figure 13 – 21. An average of the experimentally determined blade stiffness and estimated mass distributions are provide in Figures 6 through 9.

Since structural damping contributes to nearly half the total damping in each mode, it is crucial to get an accurate estimate of the structural damping. Inherent structural damping and natural frequencies of the nonrotating blades were determined by a free vibration and Moving-Block technique for the first flap and the first lag modes. For the higher flap, lag and torsional modes, it is necessary to perform a shake test. With an electrodynamic shaker tuned to the correct resonant frequency, each mode could be excited independently. The frequency response function method was used to determine the nonrotating natural frequencies for the first six modes of the model rotor system. The nonrotating modal frequencies for the lowest ten modes can be obtained cleanly by exciting the blade in the appropriate direction. Nyquist method was applied to estimate the structural damping for the excited modes. Table 2 lists the experimentally determined nonrotating blade characteristics. Again, due to dissimilarities among the blades, the measured nonrotating frequencies and dampings are slightly different for the four blades. Table 2 represents the average values for the blades.

For soft-inplane bearingless rotors, the low-damped first lag mode is most susceptible to aeromechanical instability. Therefore, one objective of the rotor test is to determine the lag mode damping under various flight conditions; i.e. hover, and forward flight up to μ=0.35. Experimental data were obtained over the range of advance ratios, shaft tilts and collective pitch settings given in Table 3. The shake-and-decay method was used to obtain the rotor response time history. A refined Moving-Block method [15], was used to determine the lag mode damping.

The test procedure involved trimming the rotor for each combination of shaft angle and collective pitch setting by adjusting the longitudinal and lateral cyclic to minimize the rotor longitudinal and lateral flapping. Then the swashplate is cyclically oscillated at the regressing lag mode frequency for about one second to excite the rotor. The swashplate is excited in lateral cyclic, θ_{1c}, with a maximum amplitude of 1°. After the rotor reaches a new steady state the excitation is cut off and the transient response is recorded for 10 seconds at a sampling frequency of 204.8 Hertz. This generates a total of 2048 data points for each test condition. From the decaying transient signal, the blade frequency spectrum was determined using a Fast Fourier Transform, then a Moving-Block technique was used to estimate the lag mode damping in the rotating frame. Figure 10 shows the rotating frame frequency spectrum obtained from the flexbeam lead-lag strain gauge for a hover test. Figure 11 shows the decaying magnitude plot from the online Moving-Block analysis. The curve represents the magitude, or envelope of the decaying lead-lag transient signal. The slope of this curve represents the equivalent damping of blade lag mode in the rotating frame. Figure 12 shows the blade natural frequencies in vacuum as predicted by the analysis. Comparison of Table 2 and Figure 12 shows the nonrotating frequencies are predicted very well.

Stability Measurement Techniques

The task of estimating the damping of any structural mode for a helicopter rotor from test data becomes complicated by the presence of undamped responses at the rotor harmonics, high measurement noise, the presence of close modes and the difficulty of exciting modes in the rotating environment. For wind tunnel testing, where damping needs to be estimated in real time, computation speed also becomes important. A refined Moving-Block analysis developed at the University of Maryland [15] was used for online damping estimation. Two refinements are introduced: recursive spectral analysis to improve frequency resolution, and a simple frequency domain interpretation for the Hanning window to reduce leakage from close modes. Moving-Block analysis is a simple and fast technique and is quite effective in estimating the damping of a mode from noisy data.

Aeroelastic Stability Analysis

In the present work, the aeromechanical stability of the bearingless rotor is calculated using refined structural modeling for the blade, a semi-empirical nonlinear aerodynamic modeling for the VR-12 airfoil, dynamic inflow, and coupled wind tunnel trim. The analysis in forward flight consists of two phases: (1) calculation of the steady rotor response, and (2) the stability calculation of the rotor perturbation equations.

The rotor dynamic analysis is based on the finite element method in space and time. The rotor blade, flexbeam, and torque tube are all assumed as elastic beams undergoing flap bending, lead-lag bending, elastic twist and axial deflections. The blade is discretized into a number of beam elements. Each element has fifteen degrees of freedom. Between elements there is continuity of displacement and slope for flap and lead-lag deflections. For axial displacement and geometric twist, there is a continuity of displacement. There are two internal nodes for axial displacement, and one for twist. The nonlinear equations of motions for the elastic bending and torsion of the elements are derived based on Hodges and Dowell equations [16].

The blade steady response solution involves the determination of time dependent blade deflections at different azimuth positions. This steady response solution is calculated using a finite element method in time formulated from the Hamilton's principle in weak form [6,7]. Fourth order Lagrangian shape functions in time are used within each time element. The blade steady response equations are nonlinear periodic equations. For the response solution, the time period of one rotor revolution is discretized into a number of time elements, and then the periodicity of response is imposed on the assembled finite element equations. To reduce computation time, these equations are transformed to the normal mode domain using the coupled natural modes of the blade. The steady response is then calculated from the resulting nonlinear algebraic equations. The hub loads are obtained by the force summation method. The blade inertia loads and the motion-induced aerodynamic forces are integrated along the span to obtain the blade loads at the root, and then summed over all the blades to obtain the rotor hub loads. Quasi-steady strip theory is used to obtain the aerodynamic loads. Noncirculatory forces based on thin airfoil theory are also included. During the blade response calculation, stall effects and unsteady aerodynamics are included using a semi-empirical method [17]. The semi-empirical formulation models the unsteady lift, drag, and pitching moment characteristics of an airfoil undergoing dynamic stall. These effects are represented in such a way as to allow progressive transition between the static stall and dynamic stall characteristics. This nonlinear aerodynamic model helps improve blade response prediction at high collective pitch and high advance ratios.

For a coupled tunnel trim solution, the trim values based on rigid flap dynamics is used as an initial guess for the first iteration. For subsequent iterations, the tunnel trim and the rotor response are calculated as one coupled solution using a modified Newton method. For a specific advance ratio μ, collective pitch setting at 3/4 radius (θ_{75}), and shaft tilt (α_s), the tunnel trim solution determines the cyclic pitch controls (θ_{1c}, θ_{1s}) necessary to minimize longitudinal and lateral flapping (β_{1c}, β_{1s}). This coupled trim procedure continues iterating until the longitudinal and lateral flapping are within a prescribed tolerance. The solution usually converges in less than five iterations. However, for extreme operating conditions such as high advance ratio, and very low or very high collective pitch settings more iterations may be required.

For stability analysis, the blade perturbation equations of motion are obtained by linearizing the blade motion about its steady deflected position. To reduce computation time, the resulting perturbation equations are transformed to the normal mode domain using the coupled free vibration characteristics of the blade about the mean deflected position. These blade perturbation equations, along with the dynamic inflow equations, are transformed to the fixed reference frame using the multiblade coordinate transformation. Unsteady aerodynamic effects are introduced approximately through a dynamic induced inflow modeling. For this, the Pitt and Peters [18] model is used.

In hover, the stability roots of the linearized perturbation equations, which involve constant coefficients, are solved using eigenvalue analysis. In forward flight, where coefficients are periodic, the equations are solved using Floquet transition matrix theory [19]. To help identify the modes in Floquet stability solution, the constant coefficient approximation method is used.

Results and Discussions

Hover

For bearingless rotor aeromechanical stability study, the lag mode stability is the most important. First of all, it is the least damped mode of all the modes of the rotor, and secondly, the low frequency

regressive lag mode is most likely to couple with the fuselage modes to cause aeromechanical instability. Therefore, in the results we present only the lag mode damping ratio in the rotating frame. The damping ratio is shown as a percentage of critical damping. Results for hover and forward flight cases are all presented in the form of rotating frame lag mode damping vs. collective pitch at 3/4 radius, θ_{75}. The nominal operating rpm of the model rotor for both hover and forward flight tests is 817 rpm. The collective pitch was varied from 0° to 10° in 2° increments. Tests were conducted for increasing and decreasing collective pitch increments. Due to small structural and control system hysterisis, upward and downward collective sweep give slightly different damping value at the same collective pitch setting. To minimize the wind tunnel wall effects for the hover test, the test section ceiling and floor were removed.

For the hover and forward flight analysis, six 15-node elements are used, two each for the main blade, flexbeam, and torque tube. Six rotor modes are used for the normalization procedure. The six modes are: the lowest two lag modes, lowest three flap modes, and the lowest torsional mode. The structural properties used for the analysis are given in Table 4.

Figures 13 and 14 show the hover collective pitch sweep correlations for shaft-fixed and shaft-free conditions, respectively. The experimentally measured damping values for blade 1 and 2 are shown the figures. The differences in blades' lag damping are due to manufacturing imperfections. As illustrated in the two figures, both theory and experiment demonstrate this particular bearingless main rotor design is stable at all collective pitch settings tested.

Forward Flight

For both shaft-fixed and shaft-free configurations, tests were conducted at advance ratios of 0.12, 0.23, and 0.35.

Figures 15 and 16 present the forward flight lag mode damping results for $\mu = 0.12$ at forward shaft tilt angle of α_s=-4°. As indicated by experimental results, the damping is relatively invariant with respect to collective pitch. Nearly half of the damping comes from the structure (1.1%) and the rest from the coulping effect of flap-lag aerodynamics. The aerodynamically generated lag damping rises from the Coriolis effect of hub precone. The UMARC was run with and without the two degree sweep back at the blade/flexbeam intersection. Theoretical analysis reveals that the sweep back contributes additional lag damping. Hence, a good bearingless rotor design should possess sufficient structural damping. Also, the design paramters such as hub precone, and blade sweep should be judiciously selected to enhance lag mode damping.

Figures 17 and 18 show correlations for collective pitch sweep at μ=0.23. The figures indicate that the analysis predicts the damping satisfactorily. It should be emphasized that model rotor like this operates at much lower Reynolds number as compared to full-sized helicopters. Full-sized helicopters typically have a blade tip Reynolds number in the 5 millions range, while this model operates at slightly less than 1/2 million. At such low Reynolds numbers, most airfoils stall near 10°. Therefore, the Beddoes/Leishman semi-empirical nonlinear stall model is included in the analysis. Including the nonlinear model showed a slight reduction in blades' flap response for collective pitch at 10° and beyond. For stability analysis, the blade equations were perturbed about the converged blade response. Even though the blade response was modified to include stall, the lag damping results did not change significantly. This because the perturbation equations did not include nonlinear stall. The two figures indicate that lag mode damping is slightly higher in the shaft-free condition. This observation is supported by the experiment. A possible explanation is that hub motions perturb the rotor inflow and induce additional rotor damping.

Figure 19 presents the measured and calculated damping for the fuselage pitching mode. The comparision shows good corelation. Figures 20 and 21 present results of shaft-fixed and shaft-free condition at μ=0.35. Again, the analysis predicts slightly higher damping for the shaft-free configuration. In Figure 21 measured damping result for both blade 1 and blade 2 are shown. The analysis assumes that the blades are identical. The blade response was calculated for one blade only using the averaged structural properties of all four blade. Therefore, it is not surprising that the calculated results represent a median response of the experimental values shown for say, blade 1 and 2. In the future it may be of interest to study the effect of dissimilar blades on aeromechanical stability. It has been hypothesized by some researchers that slight rotor imbalance may reduce aeroelastic instability.

Conclusions

A series of wind tunnel experiments were successfully conducted to investigate the aeromechanical stability of a bearingless rotor in hover and forward flight. A refined Moving-Block analysis was implemented in real time to provide a quick estimate of lag mode damping.

The model rotor and blade properties were determined by careful experimentation. These properties were used as an input to a newly refined bearingless rotor analysis code. Theoretical predictions were compared with experimental results in hover and forward flight. This test has generated a data set on the aeroelastic stability of an advanced bearingless rotor in hover and forward flight. These data can be used by researchers to help validate their theories.

Specific conclusions drawn from the present investigations are:

1. The UMARC analysis predicts the lag mode damping satisfactorily for hover and forward flight.
2. Both theory and experimental results demonstrate that this particular bearingless main rotor design is stable at all rpm and collective pitch settings tested.
3. The effects of hub motion on aeroelastic stability have been examined both experimentally and theoretically. Shaft-free condition shows slightly higher damping. Thus conventional shaft-fixed aeroelastic wind tunnel testing of new rotor designs may underpredict rotor damping.

Acknowledgements

This work was performed at the Center for Rotorcraft Education and Research Program at the University of Maryland. The work was jointly supported by NASA Ames Research Center under NASA grant NAG2-409, and by the Army Research Office under contract number DAAL-03-88-C002. The technical monitors were Mr. Khanh Nguyen and Dr. Robert Singleton, respectively. The authors appreciate Dr. Gunjit Bir for implementing the complex bearingless rotor kinematics in a consistent manner. The authors gratefully acknowledge valuable suggestions offered by Dr. Michael Torok.

References

[1] Hodges, D. H., "A Theoretical Technique for Analyzing Aeroelastic Stability of Bearingless Rotors," *AIAA Journal*, Vol. 17, No. 4, April 1979, pp. 400–407.

[2] Dawson, S., "An Experimental Investigation of the Stability of a Bearingless Model Rotor in Hover," *Journal of the American Helicopter Society*, Vol. 28, No. 4, Oct. 1983, pp. 29–34.

[3] Hooper, W. E., "Parametric Study of Aeroelastic Stability of a Bearingless Rotor," *Journal of the American Helicopter Society*, Vol. 31, No. 1, Jan. 1986, pp. 52–64.

[4] Sivaneri, N. T. and Chopra, I., "Finite Element Analysis for Bearingless Rotor Blade Aeroelasticity," *Journal of the American Helicopter Society*, Vol. 29, No. 2, April 1984, pp. 42–51.

[5] Hodges, D. H., Hopkins, A. S., Kunz, D. L., and Hinnant, H. E., "Introduction to GRASP – General Rotorcraft Aeromechanical Stability Program – A Modern Approach to Rotorcraft Modeling," *Journal of the American Helicopter Society*, Vol. 32, No. 2, April 1987, pp. 78–90.

[6] Panda, B. and Chopra, I., "Dynamics of Composite Rotor Blades in Forward Flight with Application of Finite Element in Time," *Vertica*, Vol. 11, No. 1/2, 1987, pp. 187–209.

[7] Panda, B. and Chopra, I., "Flap–Lag–Torsion Stability in Forward Flight," *Journal of the American Helicopter Society*, Vol. 30, No. 4, Oct. 1985, pp. 30–39.

[8] Birs, G. S. and Chopra, I., "Gust Response of Hingeless Rotors," *Journal of American Helicopter Society*, Vol. 31, No. 2, April 1986, pp. 33–46.

[9] Jang, J. and Chopra, I., "Ground and Air Resonance of Bearingless Rotors in Hover," *Journal of the American Helicopter Society*, Vol. 33, No. 3, July 1988, pp. 20–29.

[10] Jang, J. and Chopra, I., "Air Resonance of an Advanced Bearingless Rotor in Forward Flight," *Second International Rotorcraft Basic Research Conference*, College Park, Maryland, Feb. 1988.

[11] Wang, J. M., Chopra, I., Samak, D. K., Green, M. and Graham, T., "Theoretical and Experimental Investigation of the Aeroelastic Stability of an Advanced Bearingless Rotor in Hover and Forward Flight," presented at the *American Helicopter Society National Specialists' Meeting on Rotorcraft Dynamics*, Arlington, Texas, Nov. 1989.

[12] Wang, J. M., Jang, J. and Chopra, I., "Air Resonance Stability of Hingeless Rotors in Forward Flight," *Vertica*, Vol. 14, No. 2, 1990, pp. 123–136.

[13] Torok, M. S. and Chopra, I, "A Coupled Rotor Aeroelastic Analysis Utilizing Nonlinear Aerodynamics and Refined Wake Modeling," *Vertica*, Vol. 13, No. 2, 1989.

[14] Bir., G., Chopra, I. and Khanh, N., "Development of UMARC (University of Maryland Advanced Rotorcraft Code)," presented at the *46th Annual National Forum of the American Helicopter Society*, Washington, D. C., May 1990.

[15] Tasker, F. A. and Chopra, I., "Assesment of Transient Testing Techniques for Rotor Stability Testing," *Journal of the American Helicopter Society*, Vol. 35, No. 1, pp. 39–50.

[16] Hodges, D. H. and Dowell, E. H., "Nonlinear Equations of Motion for the Elastic Bending and Torsion of Twisted Nonuniform Rotor Blades," NASA TN–D 7818, Dec. 1974.

[17] Leishman, J. G. and Beddoes, T. S., "A Semi-Empirical Model for Dynamic Stall," *Journal of the American Helicopter Society*, Vol. 34, No. 3, July 1989, pp. 3–17.

[18] Pitt, D. M. and Peters, D. A., "Theoretical Prediction of Dynamic Inflow Derivatives," *Vertica*, Vol. 5, No. 1, 1981, pp. 21–34.

[19] Peters, D. A. and Hohenemser, K. H., "Application of the Floquet Transition Matrix to Problems of Lifting Rotor Stability," *Journal of the American Helicopter Society*, Vol. 16, No. 2, April 1971, pp. 25–33.

Table 1 Rotor Geometry

Number of blades, b	4
Rotor radius, R	3.0 ft
Blade chord, c	.254 ft
Blade airfoil,	VR-12
Rotor Solidity, $bc/\pi R$	0.1079
Blade twist (linear)	-8°
Blade pretwist	14°
Blade sweptback	-2°
Hub precone	4°
Lock number	5.673
Body roll mode freq.	12.5 Hz
Body pitch mode freq	8.6 Hz
Body roll mode damping	2.5 %
Body pitch mode damping	2.5%

Table 2 Measured Nonrotating characteristics

natural mode	natural frequency (hz)	structural damping (%)
1st flap	3.13	4.8
1st lag	7.90	1.1
2nd flap	18.52	3.8
3rd flap	55.56	2.8
1st torsion	60.05	5.0
2nd lag	73.94	4.0

Table 3 Range of test parameters

Parameter	Test Values
Advance ratio, μ	0.0, 0.12, 0.23, 0.35
Shaft angles, α_s	0°, -4°, -8°
Collective pitch angles, θ_c	0°, 2°, 4°, 6°, 8° ,10°
Nominal rotor speed	817 rpm

Table 4 Bearingless Model Structural Properties Used for Analysis

Element	Flapwise $\frac{EI_y}{m_0\Omega^2R^4}$	Chordwise $\frac{EI_z}{m_0\Omega^2R^4}$	Torsion $\frac{GJ}{m_0\Omega^2R^4}$	Mass $\frac{m}{m_0}$	Radius of Gyration $\frac{k_m}{R}$	Length $\frac{\ell}{R}$
1	.00301	.05367	.00282	.8797	.02236	.25
2	.00376	.06440	.00338	.8797	.02362	.5625
3	.00015	.00537	.00006	.1100	.00548	.0417
4	.00150	.01073	.00068	.4400	.00583	.125
5	.00543	.00915	.00338	.3956	.00728	.0417
6	.01282	.01368	.00676	.5516	.00933	.1232

Blade = element 1 & 2
Flexbeam = element 3 & 4
Torque tube = element 5 & 6
Ω = 85.556 rad/sec
m_0 = .00546 slug/ft = .000455 slug/in

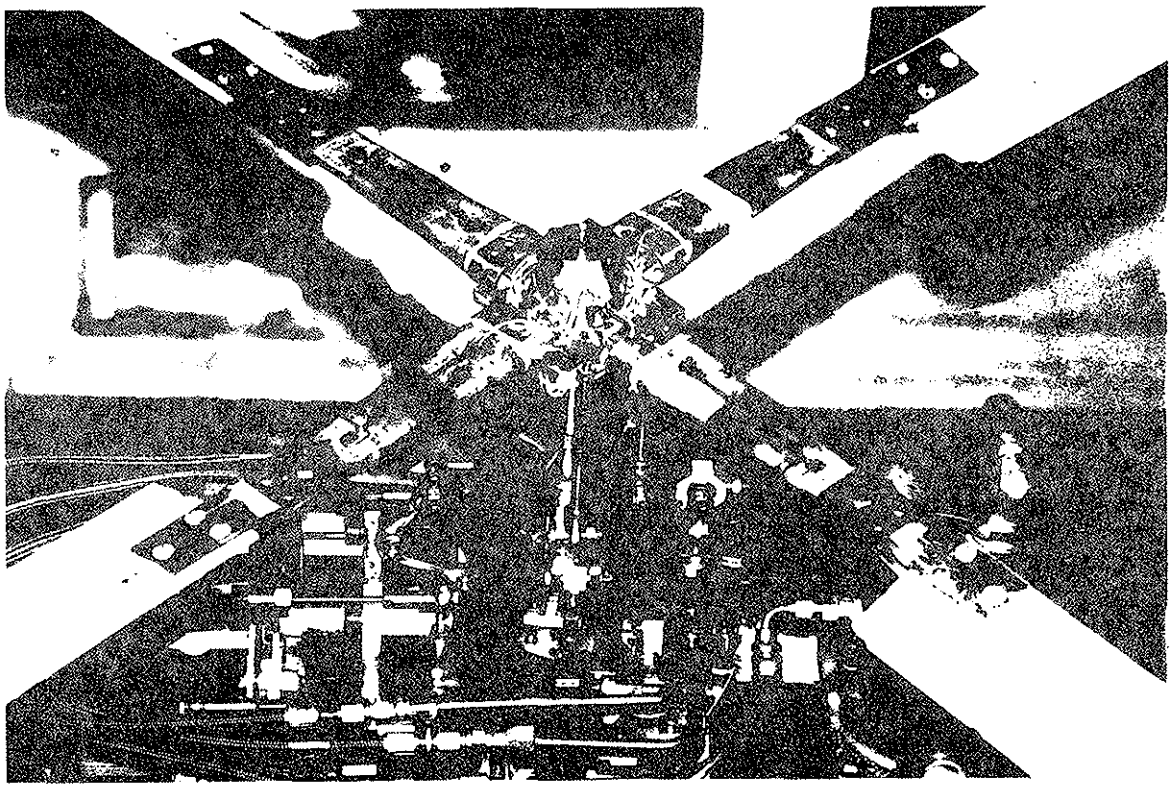

Figure 1 The 1/8th Froude scaled Boeing ITR bearingless rotor during aeromechanical testing at the Glenn L. Martin Wind Tunnel of University of Maryland.

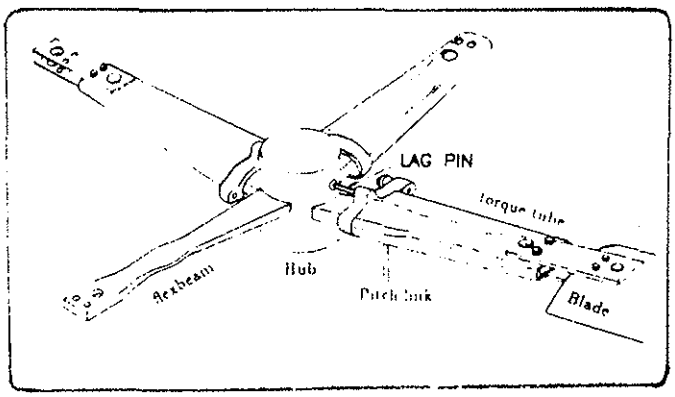

Figure 2 Boeing Vertol's ITR bearingless rotor design.

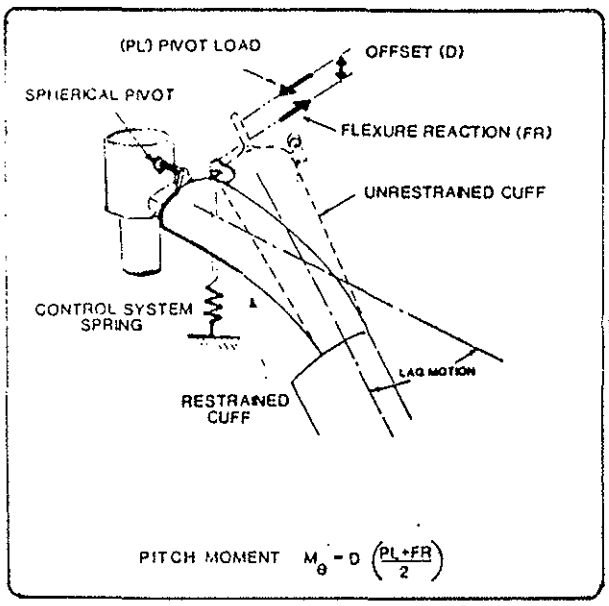

Figure 4 The lag pin design provides a favorable lag back/nose up pitch-lag coupling to improve lag mode stability. M_θ is feathering moment generated due to lead-lag.

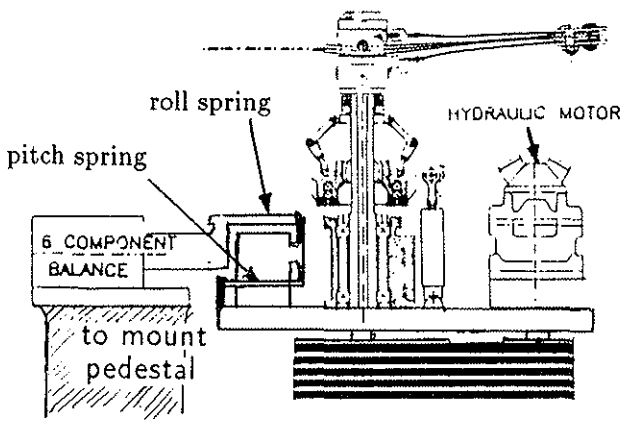

Figure 3 The model rotor rig.

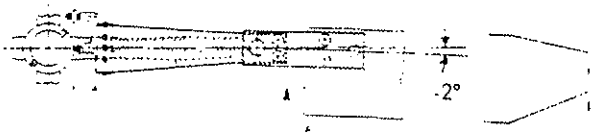

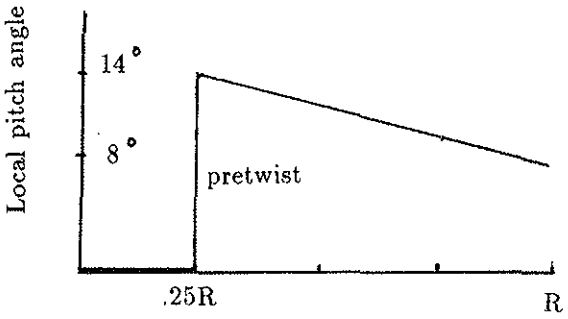

Figure 5 Blade twist distribution.

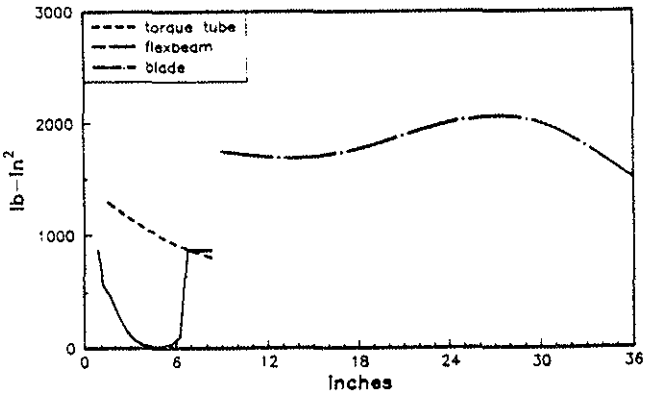

Figure 6 Experimentally determined model blade flap stiffness. (Averaged over 4 blades.)

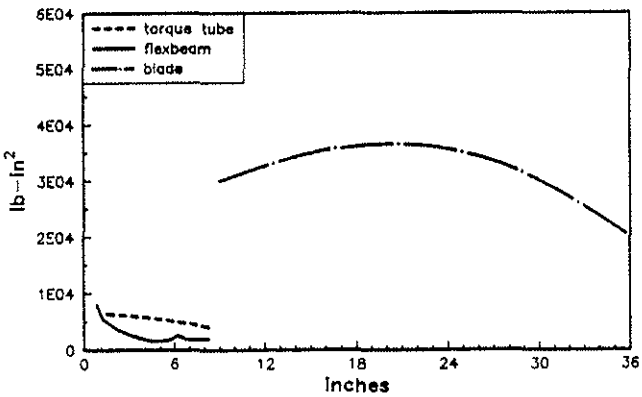

Figure 7 Experimentally determined model blade lead-lag stiffness. (Averaged over 4 blades.)

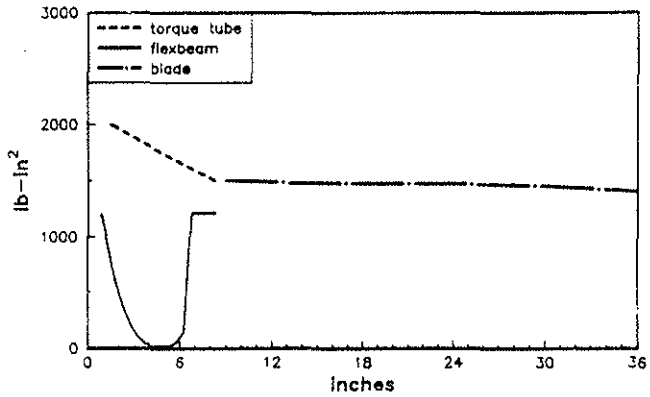

Figure 8 Experimentally determined model blade torsional stiffness. (Averaged over 4 blades.)

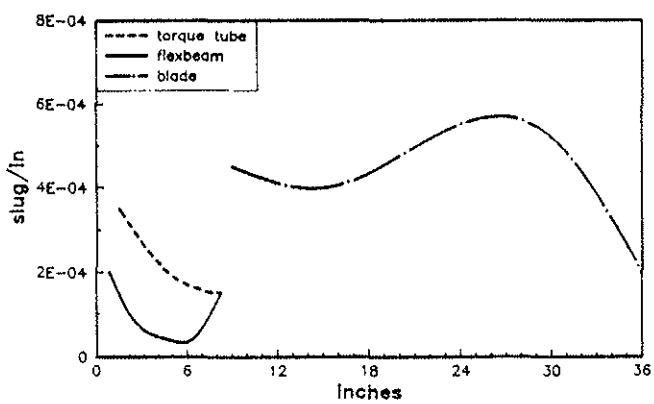

Figure 9 Estimated model blade mass distribution.

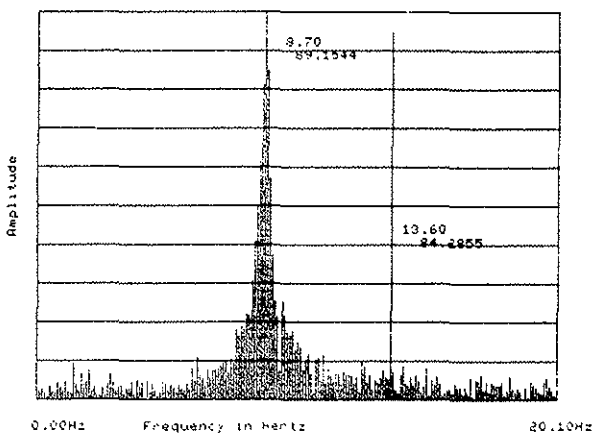

Figure 10 Rotating frame frequency spectrum from blade number 1's lead-lag strain gauge. In hover, rpm=817, θ_{75}=0°.

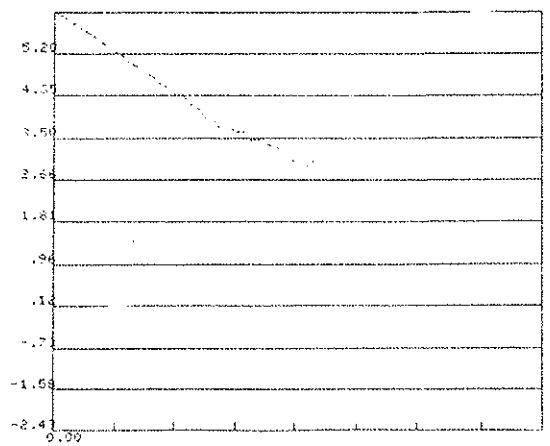

Figure 11 Moving-Block result for the lag mode response at the lag frequency shown in Fig. 10.

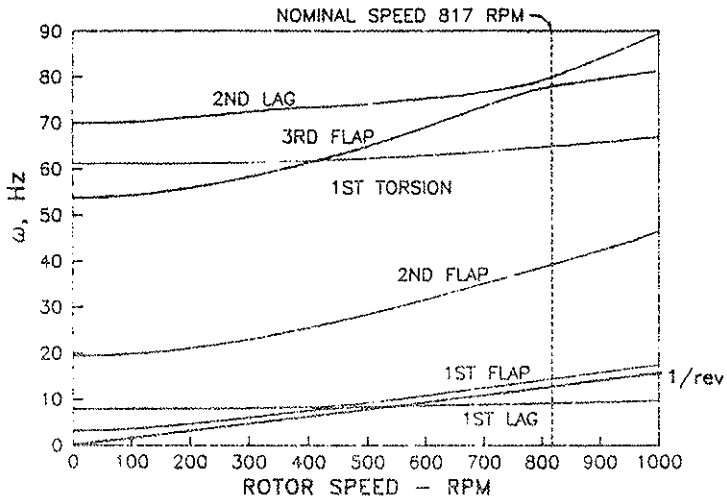

Figure 12 Fan diagram of blade natural frequencies vs. rotor speed at θ_{75}=0°, in vacuum.

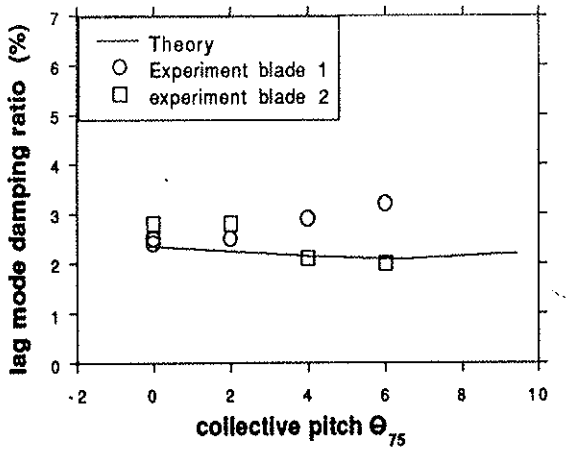

Figure 13 Hover, rpm=817, shaft-fixed.

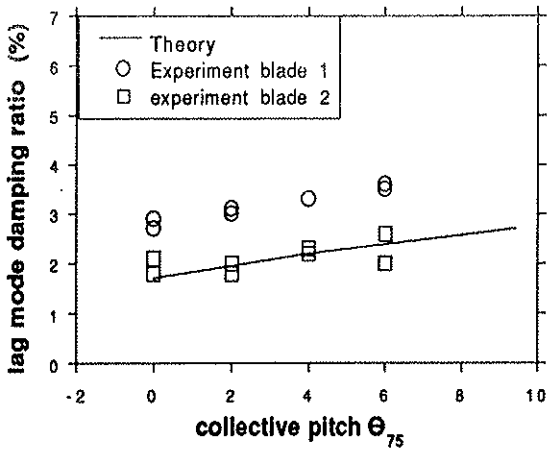

Figure 14 Hover, rpm=817, shaft-free

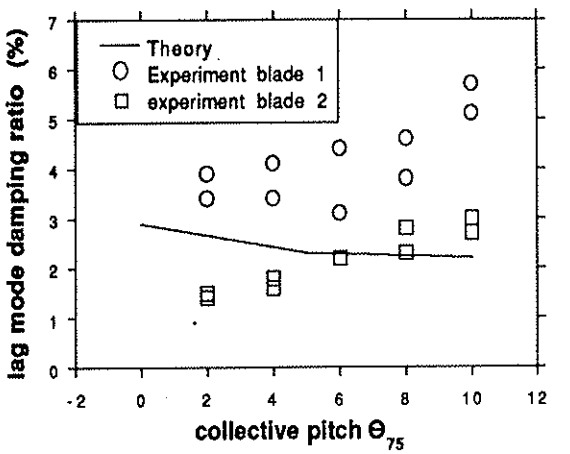

Figure 15 μ=0.12, α_s=−4° (forward tilt), shaft-fixed.

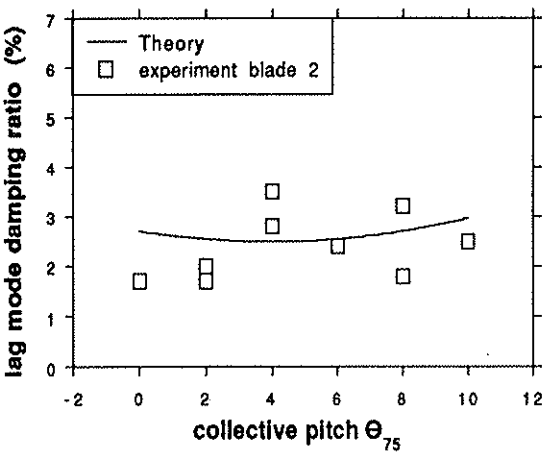

Figure 16 μ=0.12, α_s=−4° (forward tilt), shaft-free.

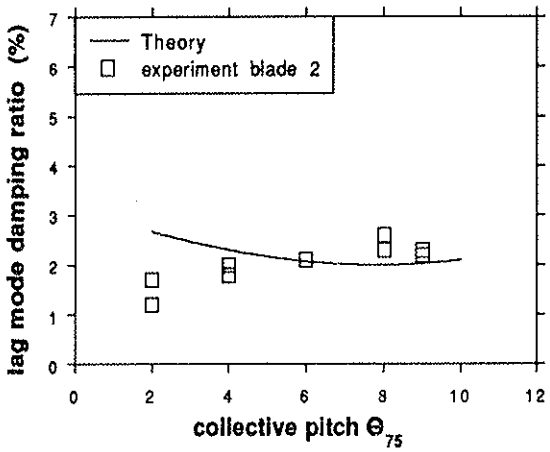

Figure 17 μ=0.23, α_s=−4° (forward tilt), shaft-fixed.

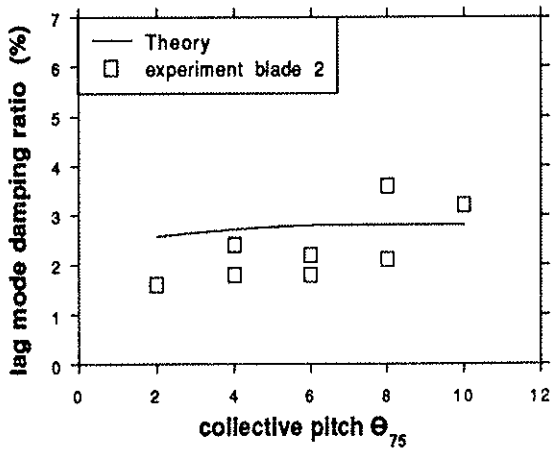

Figure 18 μ=0.23, α_s=−4° (forward tilt), shaft-free.

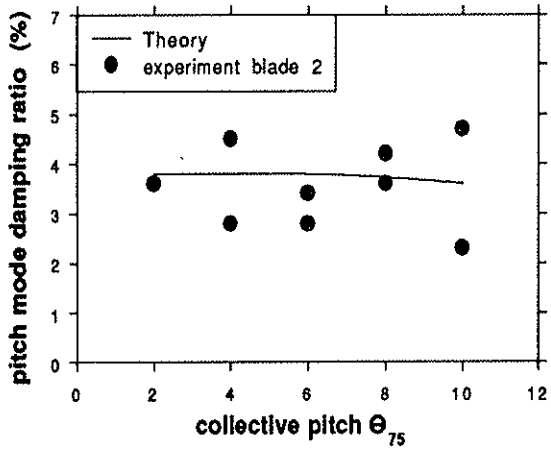

Figure 19 μ=0.23, α_s=−4° (forward tilt), shaft-free fuselage pitch mode damping.

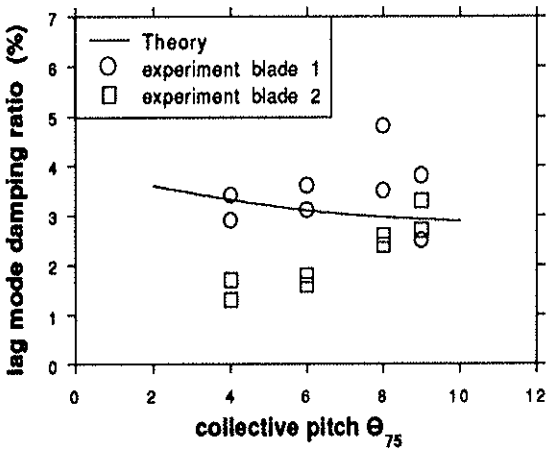

Figure 20 μ=0.35, α_s=−8° (forward tilt), shaft-fixed.

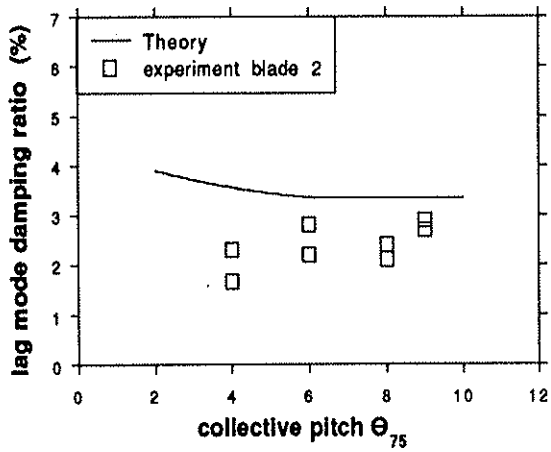

Figure 21 μ=0.35, α_s=−8° (forward tilt), shaft-free.